Oxidation and anion lattice defect signatures of hypostoichiometric lanthanide-doped UO_2

Travis Olds, **Sam Karcher**, Kyle Kriegsman, Xiaofeng Guo, John McCloy

30th Spent Fuel Workshop

14 November 2019

Doping and sintering

- 1, 5 at. % of Ce, Nd or Yb

Trivalent dopants hinder U_3O_8 formation slowing UO_2 oxidation and dissolution

XRD, EPMA

Raman

- Oxidation from $(U_{1-y}M_y)O_{2-x}$ to $(U_{1-y}M_y)O_2$

Hypostoichiometry induced by doping

TGA and DSC

UO2 Defects

UO_2 [U^{IV}]→ U_4O_9/U_3O_7 [mixed]→ U_3O_8 [U^{VI}]

U^{IV} = stable ✓

U^{VI} = soluble ✗ $(UO_2)^{2+}$

Reduced cuboctahedra formation limits shear transformation associated with the transition from crumpled α-U_4O_9 sheet structure → U_3O_8 sheet structure

Randomly distributed **trivalent cations** forces U^{IV} → U^{VI}, **inhibiting cuboctahedra** formation

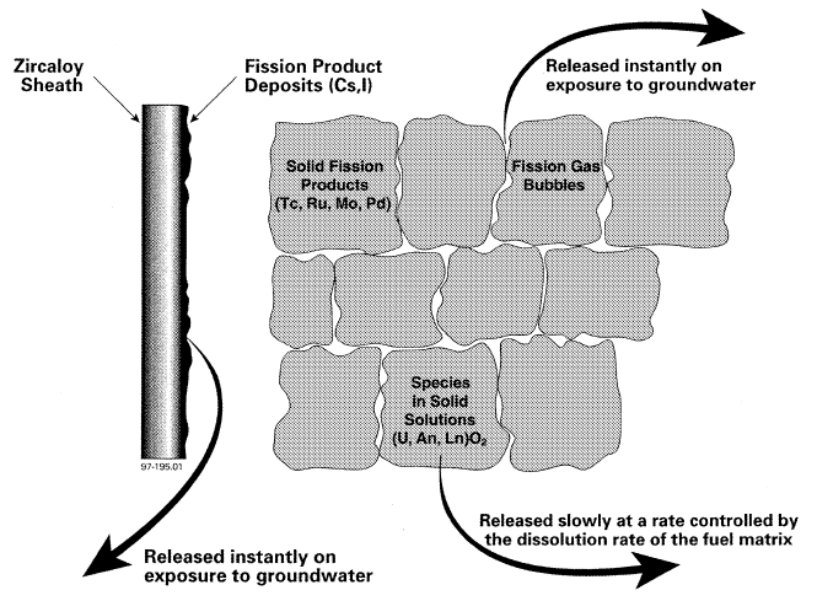

Cuboctahedral cluster

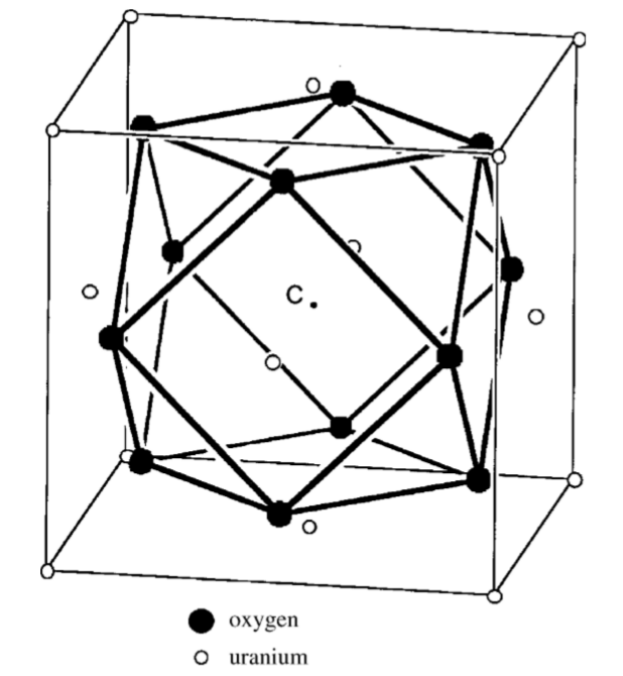

Willis 2:2:2 cluster

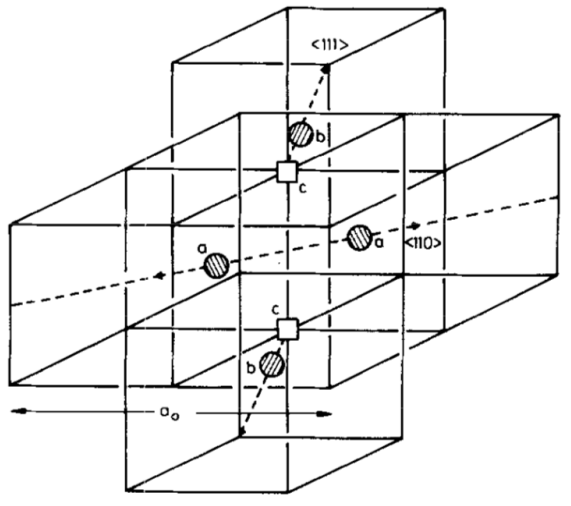

Shoesmith, D. W., & D.W, S. (2000). Fuel corrosion processes under waste disposal conditions. *Journal of Nuclear Materials*, *282*(1), 1–31. https://doi.org/10.1016/s0022-3115(00)00392-5

Murray, A. D., & Willis, B. T. M. (1990). A neutron diffraction study of anion clusters in nonstoichiometric uranium dioxide. *Journal of Solid State Chemistry*, *84*(1), 52–57. https://doi.org/10.1016/0022-4596(90)90183-X

Garrido, F., Ibberson, R. M., Nowicki, L., & Willis, B. T. M. (2003). Cuboctahedral oxygen clusters in U3O7. *Journal of Nuclear Materials*, *322*(1), 87–89. https://doi.org/10.1016/S0022-3115(03)00318-0

Doped UO_2 Synthesis

- Uranyl nitrate (+ RE-nitrate) + NH_4OH → ammonium diuranate (yellowcake)
- Filter, rinse and dry
- Calcine @ 800° C → U_3O_8
- Mill, press
- Reduce U^{VI} to U^{IV} in UO_2 by sintering at 1690° C in 4%H-96%Ar

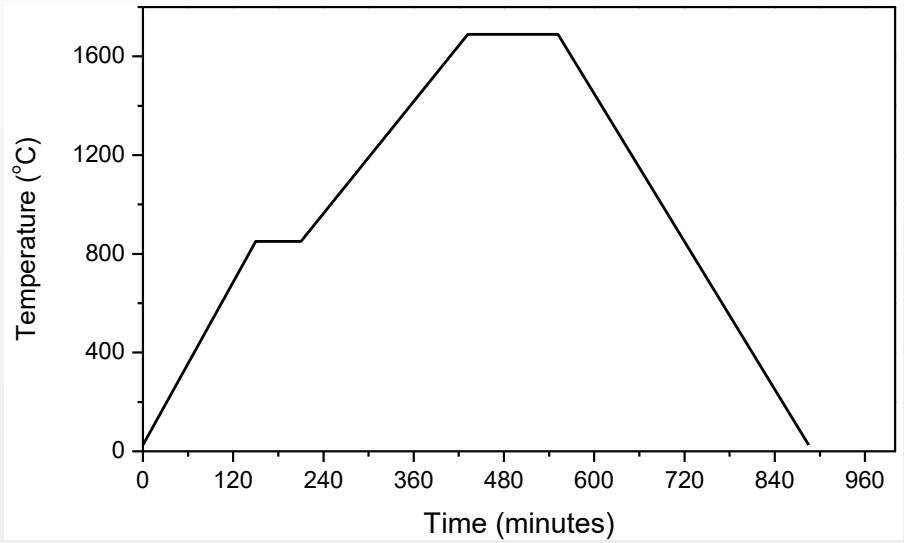

$UO_2(NO_3)_2$ *(aq)* + $(NH_4)OH \rightarrow (NH_4)_2U_2O_7$
$(NH_4)_2U_2O_7 \rightarrow$ (calcine 800° C) $\rightarrow U_3O_8 \rightarrow$ (sinter 1690° C) $\rightarrow UO_2$

Uranyl nitrate (left)
ADU/yellowcake (middle)
Calcined U_3O_8 (right)

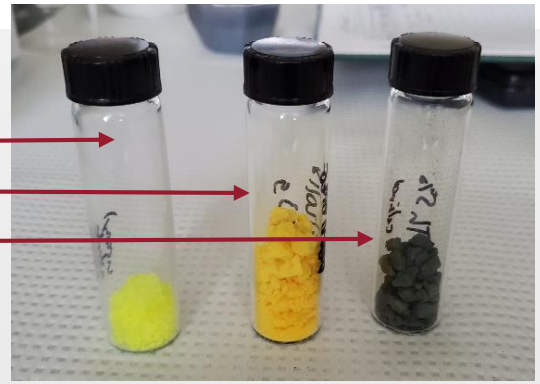

Dopant	Ce^{III}	Ce^{IV}	Nd^{III}	Yb^{III}	U^{IV}	U^{V}	U^{VI}
Ionic radius (Å)	0.97	0.985	1.109	1.143	1.00	0.84	0.86

Shannon, R. D. Revised effective ionic radii in halides and chalcogenides. *Acta Crystallogr.* 751 (1976). doi:10.1107/S0567739476001551

XRD and EPMA

Dopant	Ce^{III}	Ce^{IV}	Nd^{III}	Yb^{III}	U^{IV}	U^{V}	U^{VI}
Ionic radius (Å)	0.143	0.97	1.109	0.985	1.00	0.84	0.86

Dopant	Pure	Ce	Nd	Yb
Composition	$UO_{2.03}$	$U_{0.988}Ce_{0.012}O_{1.98}$ $U_{0.947}Ce_{0.053}O_{1.96}$	$U_{0.985}Nd_{0.015}O_{1.97}$ $U_{0.948}Nd_{0.052}O_{1.98}$	$U_{0.982}Yb_{0.018}O_{1.98}$ $U_{0.947}Yb_{0.053}O_{1.92}$

Dopant	Ce	Nd	Yb
da/dy (Å)	-0.031	-0.203	-0.093

Indicates only Ce^{III} is present

Ce^{IV} da/dy = -0.0693
Ce^{III} da/dy = -0.039

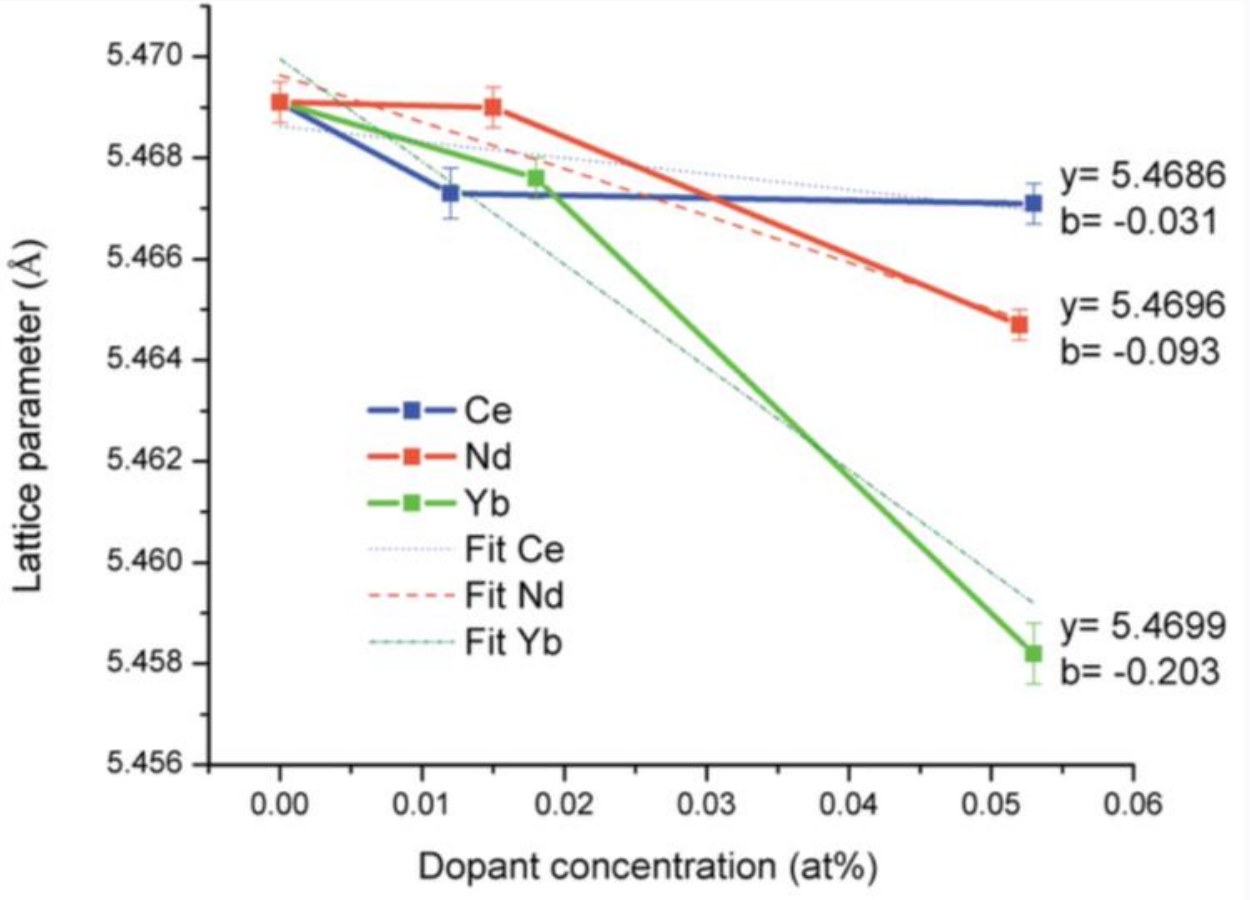

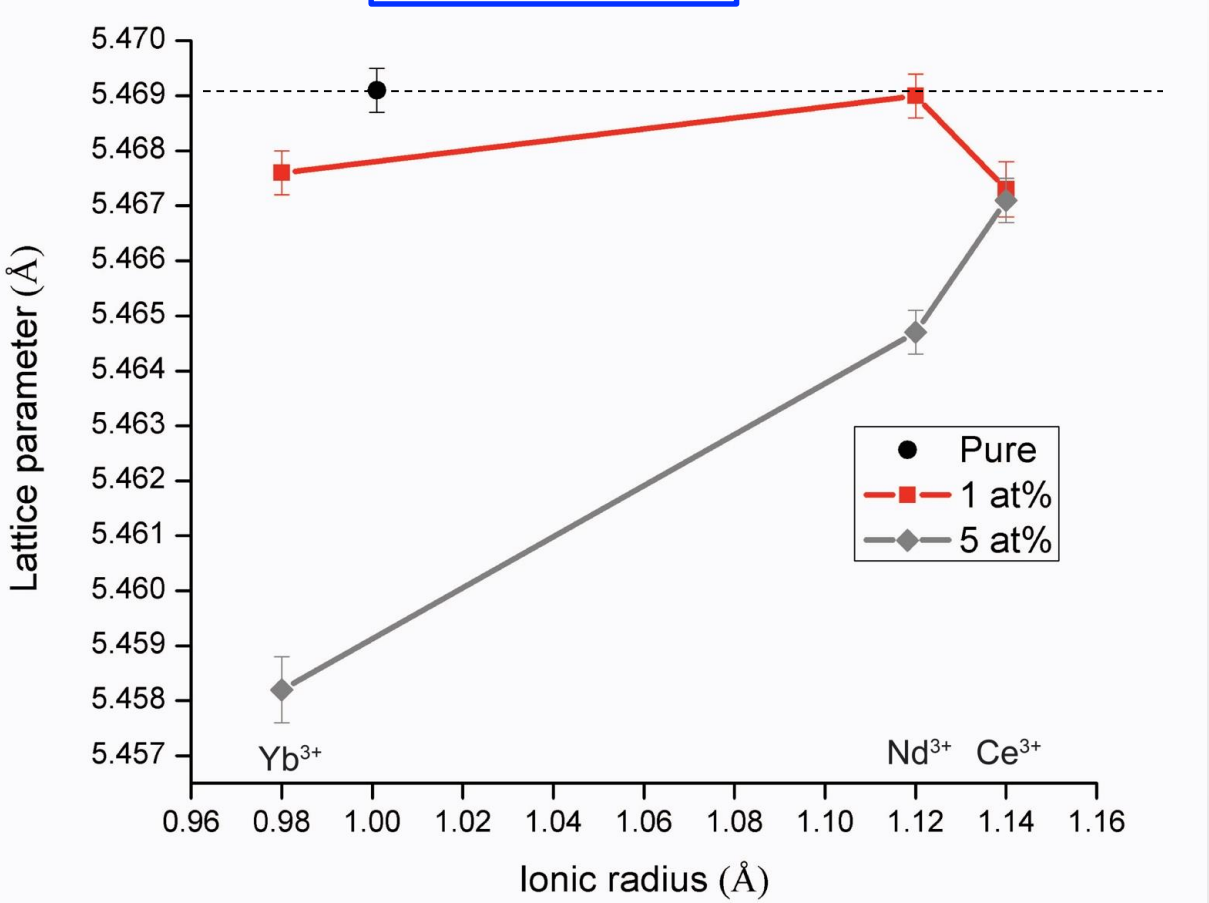

Raman

Freshly sintered vs. oxidized
Raman spectra (455 nm)

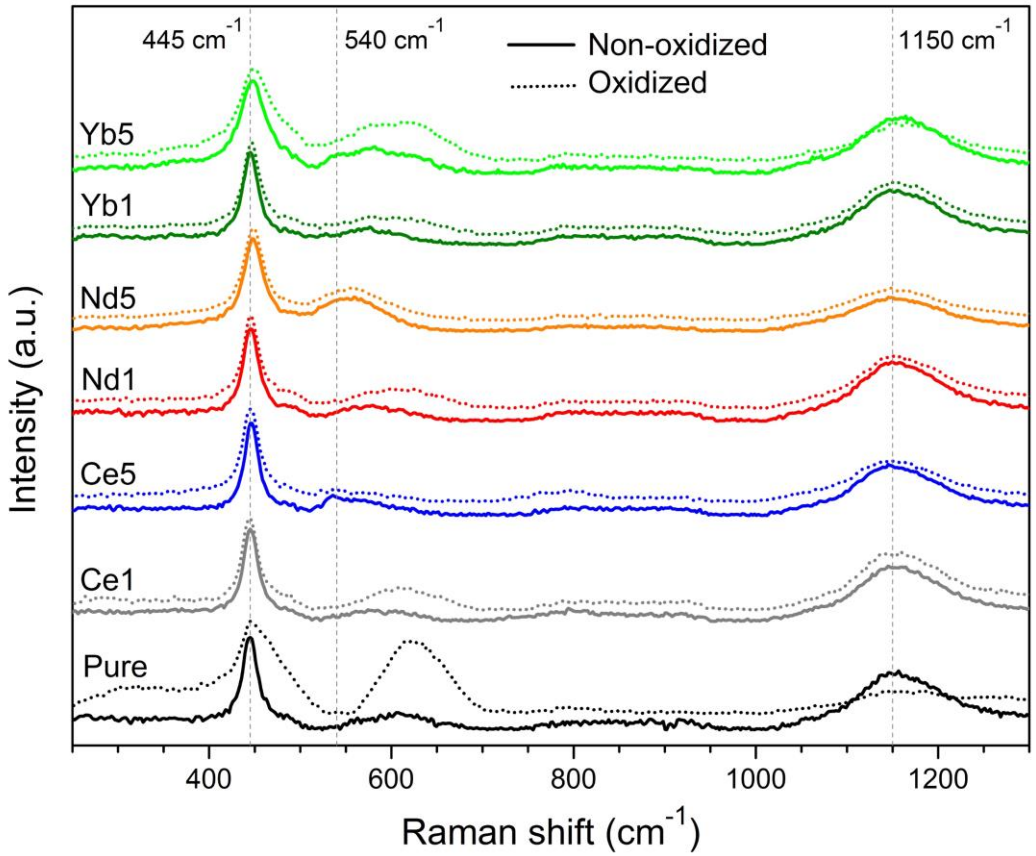

Freshly sintered vs. oxidized
Raman spectra (785 nm)

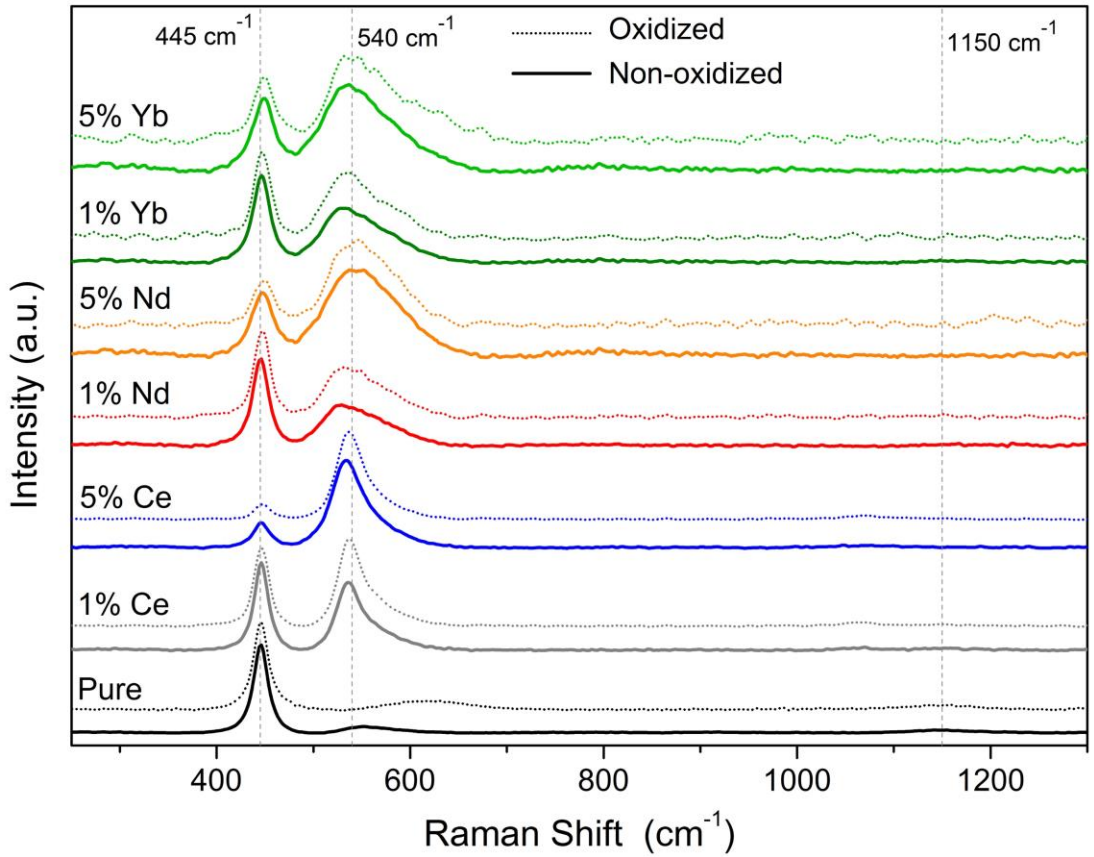

Blue laser provides better sensitivity to 2LO

Red laser provides better sensitivity in defect band region

“oxidized” samples reacted in Parr vessel at 180° C in 10 mL DI water for 18 h

Raman

Freshly sintered vs. oxidized
Raman spectra (455 nm)

Freshly sintered vs. oxidized
Raman spectra (785 nm)

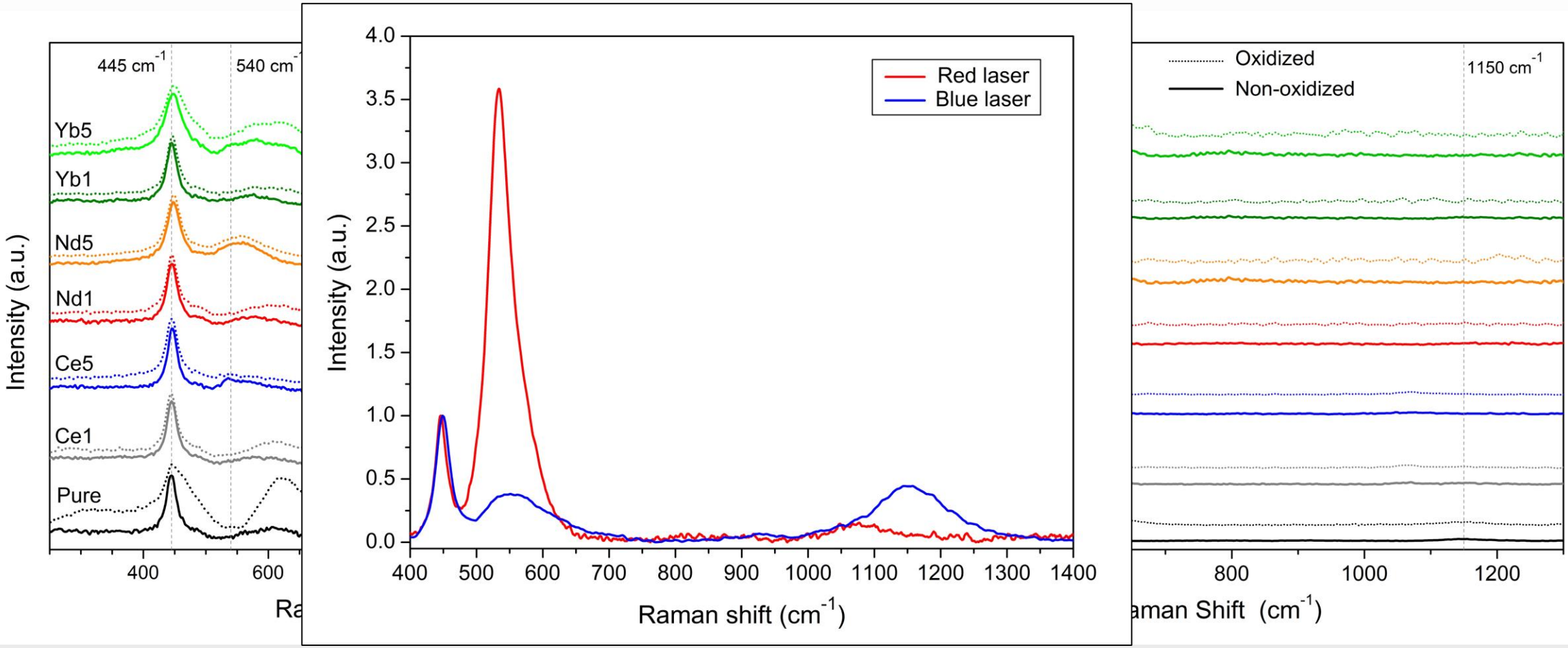

Blue laser provides better sensitivity to 2LO

Red laser provides better sensitivity in defect band region

Raman – Pure UO_2

Pure UO_2 - one Raman mode:

T_{2g} (445 cm^{-1}) symmetric U^{IV}-O stretching mode

Lattice defects cause a breakdown in symmetry, broad defect band in 500-700 cm^{-1} range to appear

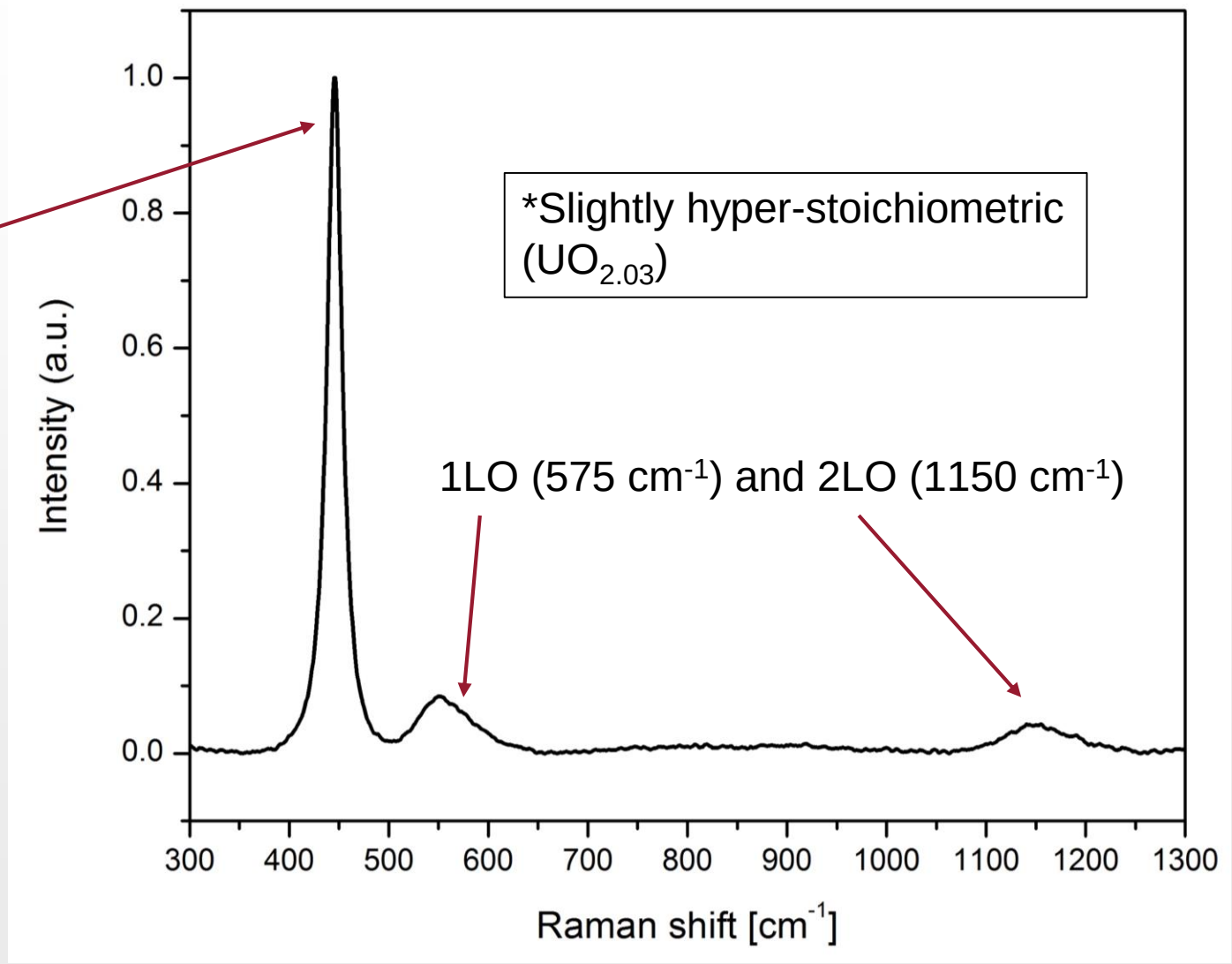

Measured with red laser

T_{2g} position

Broadening of T_{2g} band

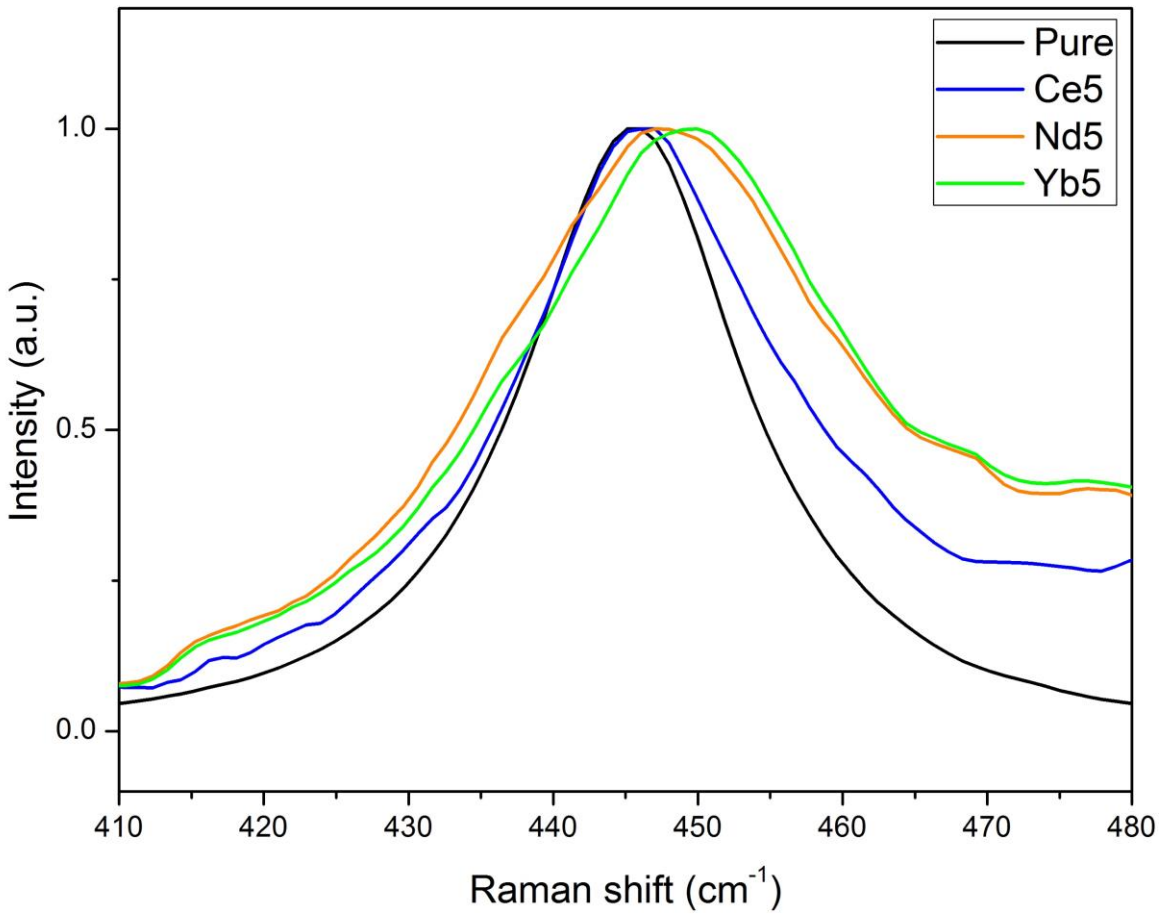

Shift in T_{2g} band positions (785nm laser)

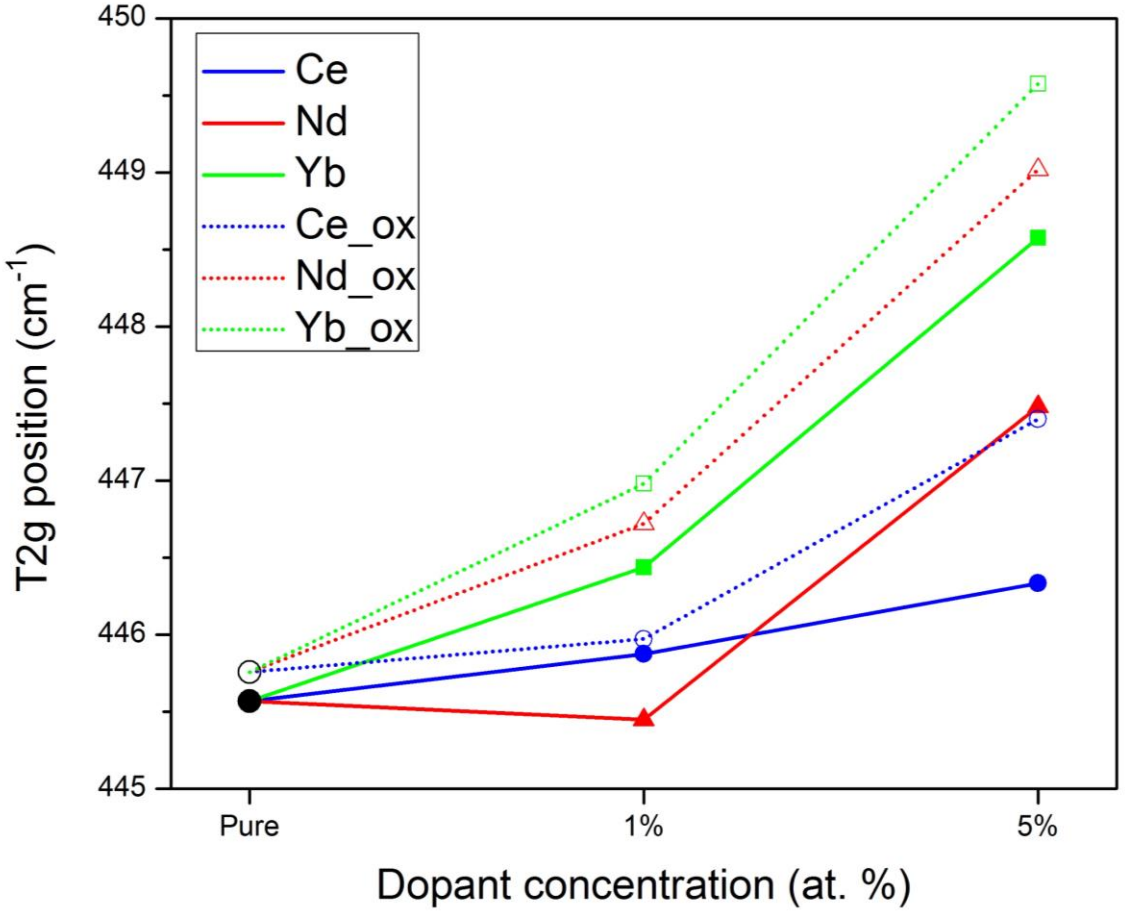

Upward shift of T_{2g} associated with increasing O_i formation and U^V formation from 3+ doping

Measured with red laser

T_{2g} position and lattice parameter

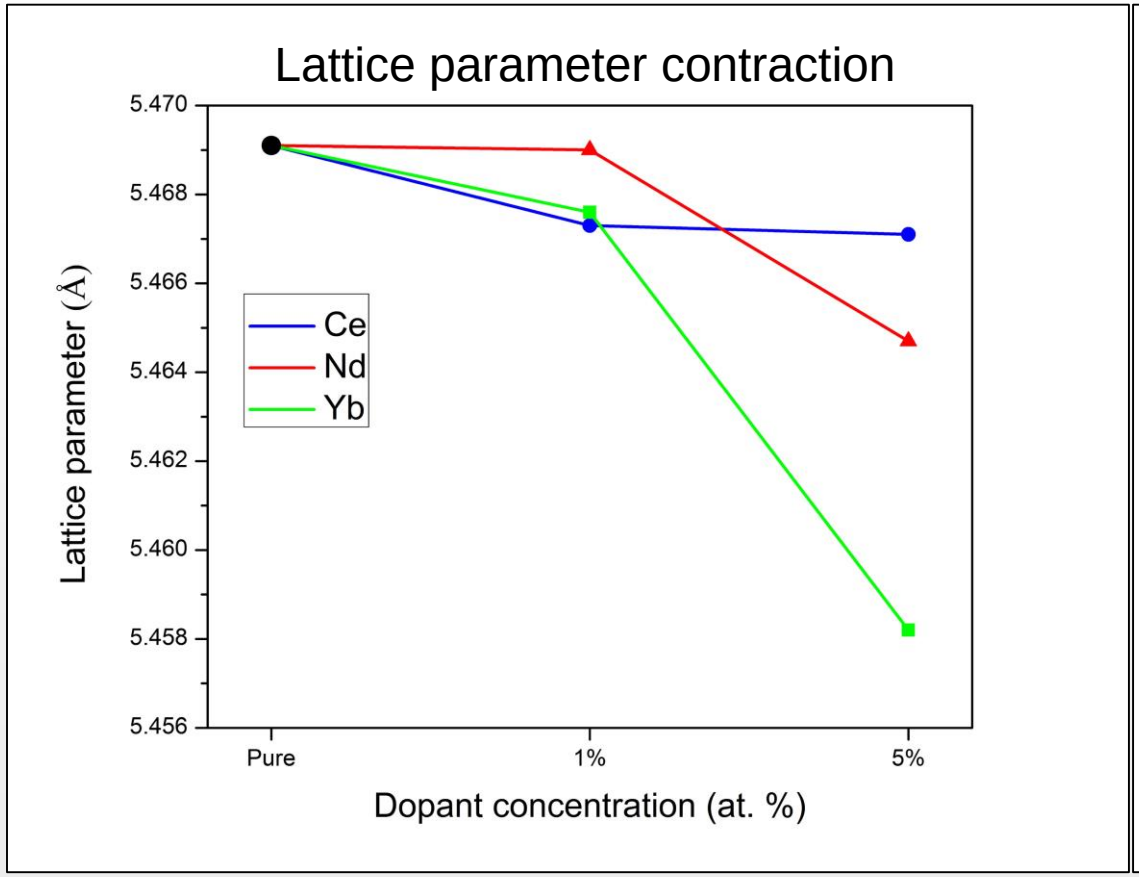

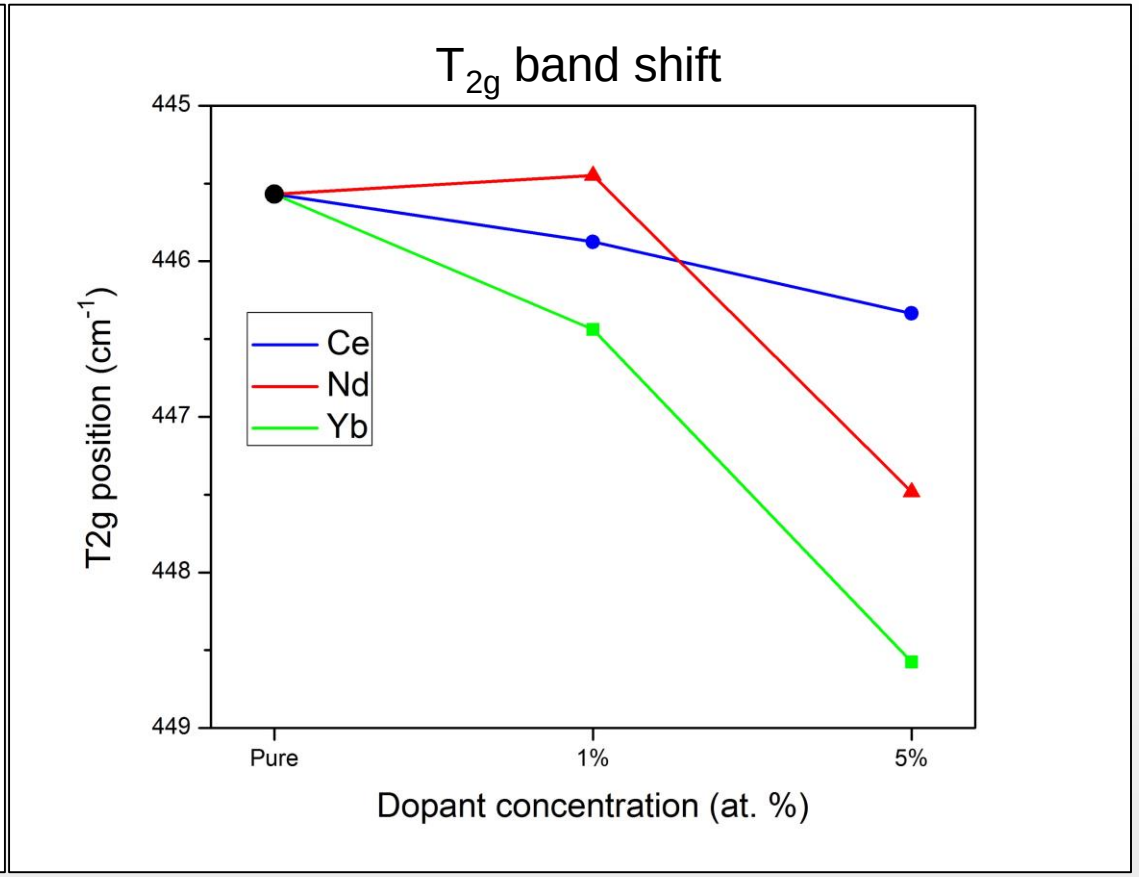

Measured with red laser

Raman – defect bands

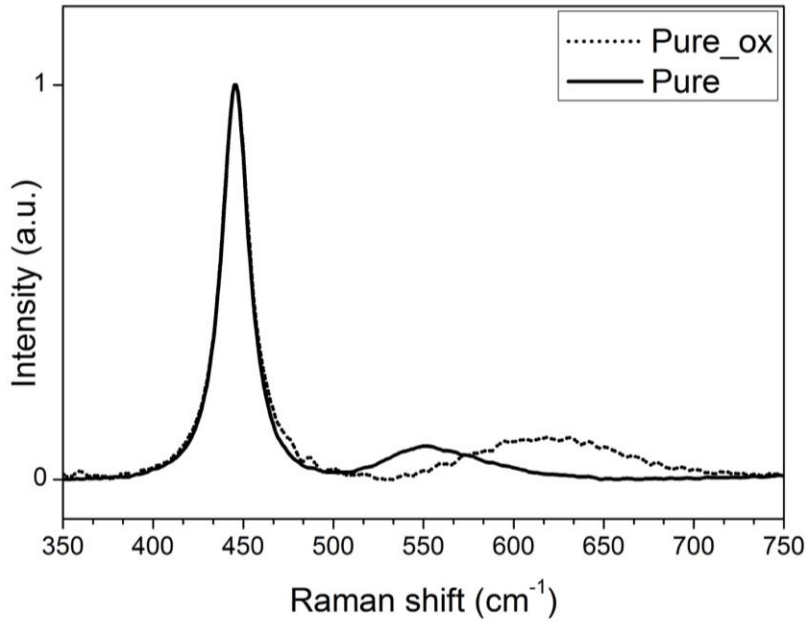

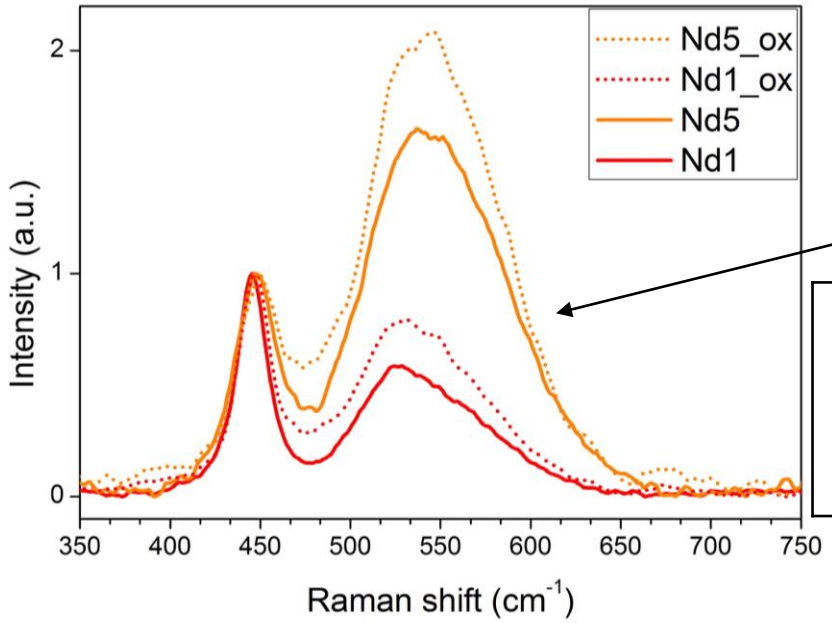

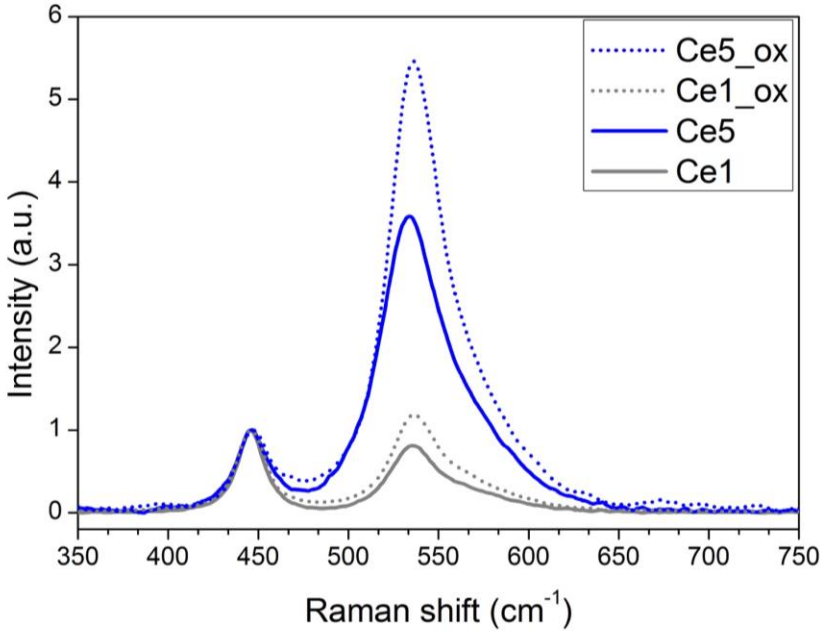

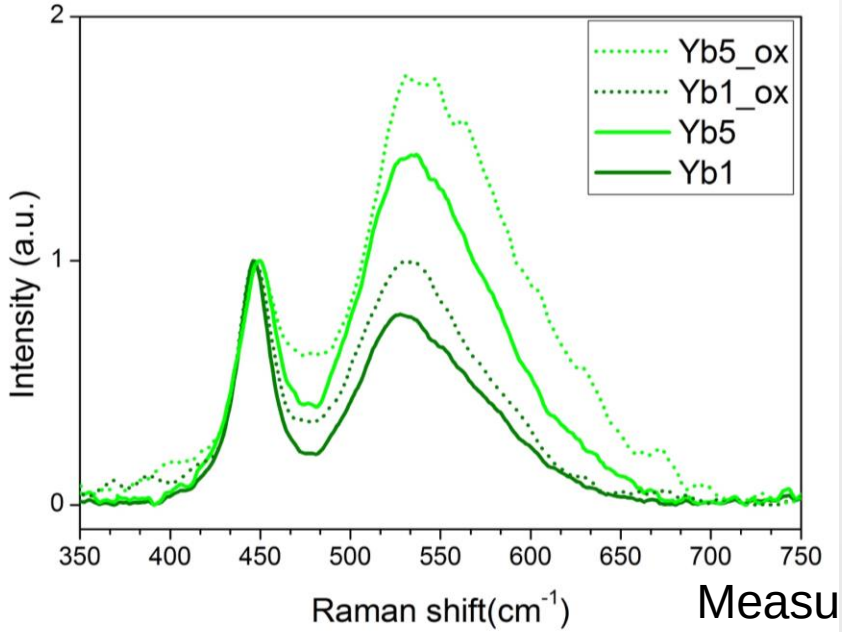

defect bands:

540 cm^{-1}	O vacancies (V_O)
575 cm^{-1}	Anion defects, reduced symmetry
640 cm^{-1}	Cuboctahedral O clusters (U_4O_9)

T_{2g}/V_O ratio used as an indication of oxygen vacancies introduces by RE^{III} doping

Measured with red laser

Raman – Defect band fitting

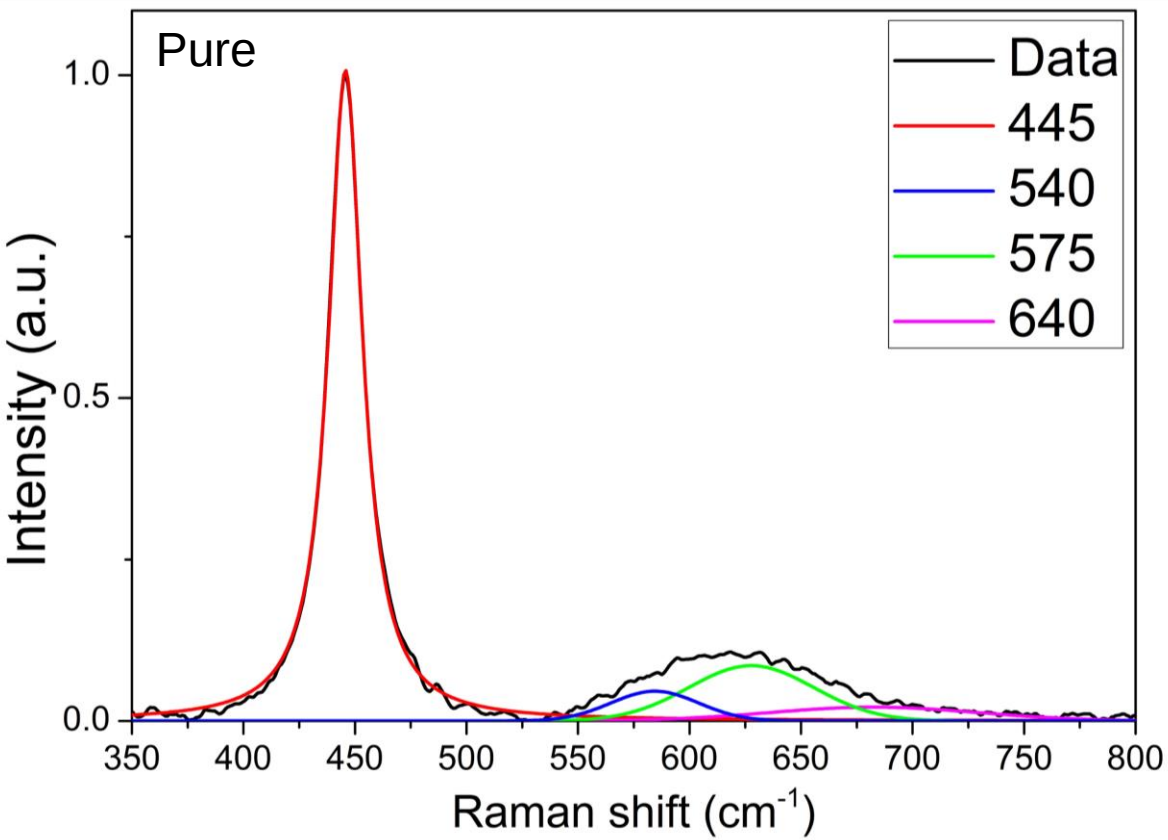

540 cm^{-1}	O vacancies (V_O)
575 cm^{-1}	Anion defects, reduced symmetry
640 cm^{-1}	Cuboctahedral O clusters (U_4O_9)

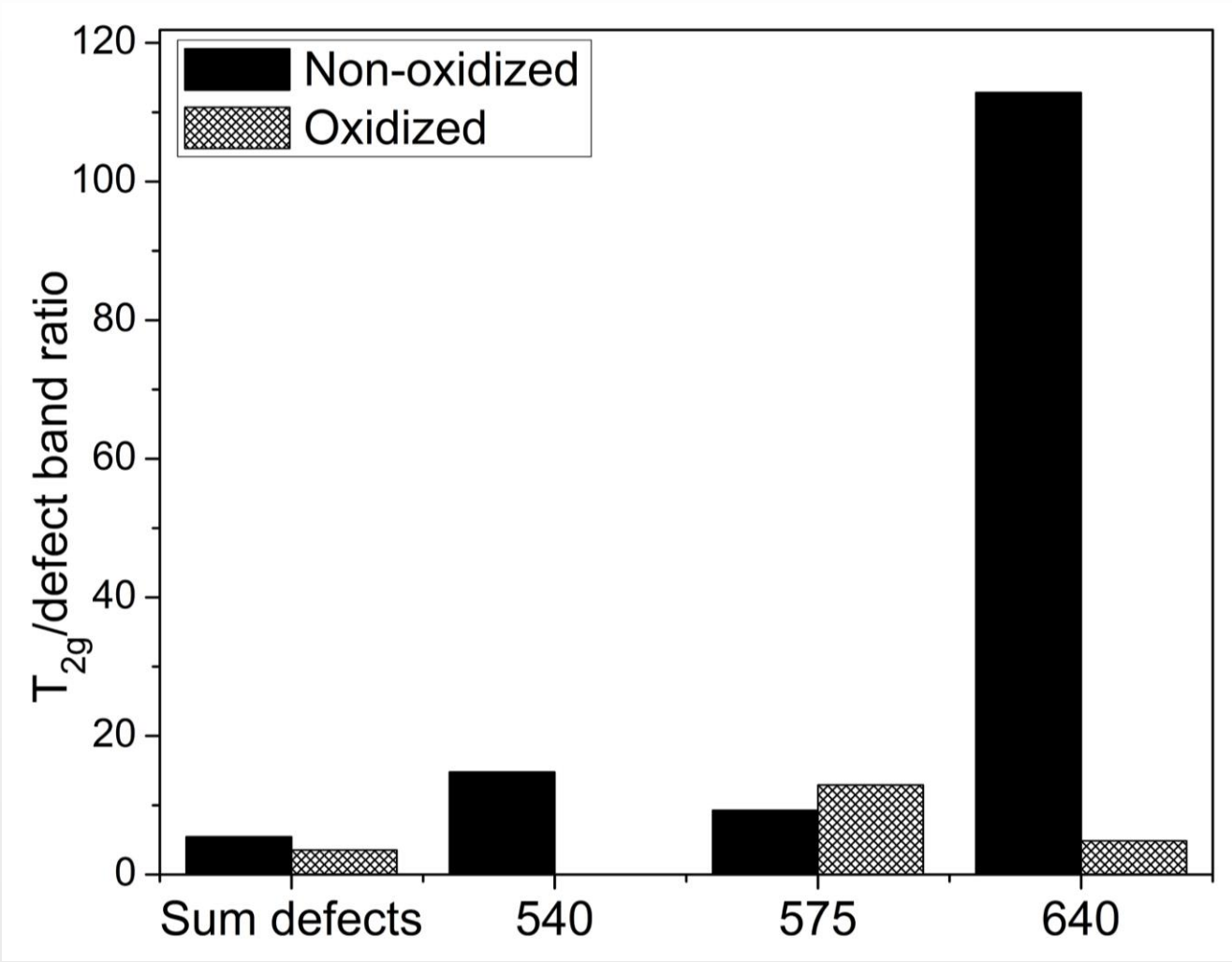

Measured with red laser

Raman - T_{2g}/area sum of defect bands

Sum of the area of 3 defect bands

Pure samples have much **fewer defects than doped samples**.
Defects **increase** as we increase **dopant concentration** and after **oxidation**

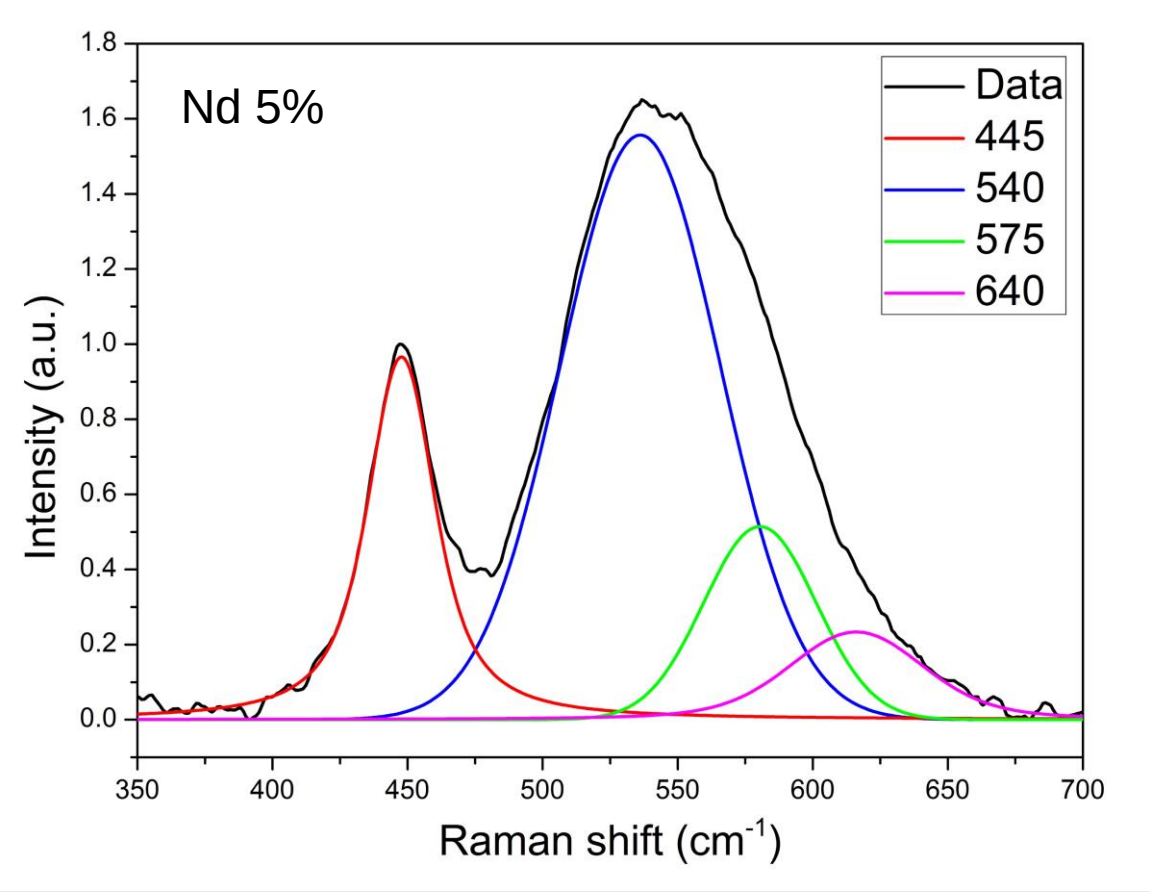

As ratio ↓ overall defects ↑

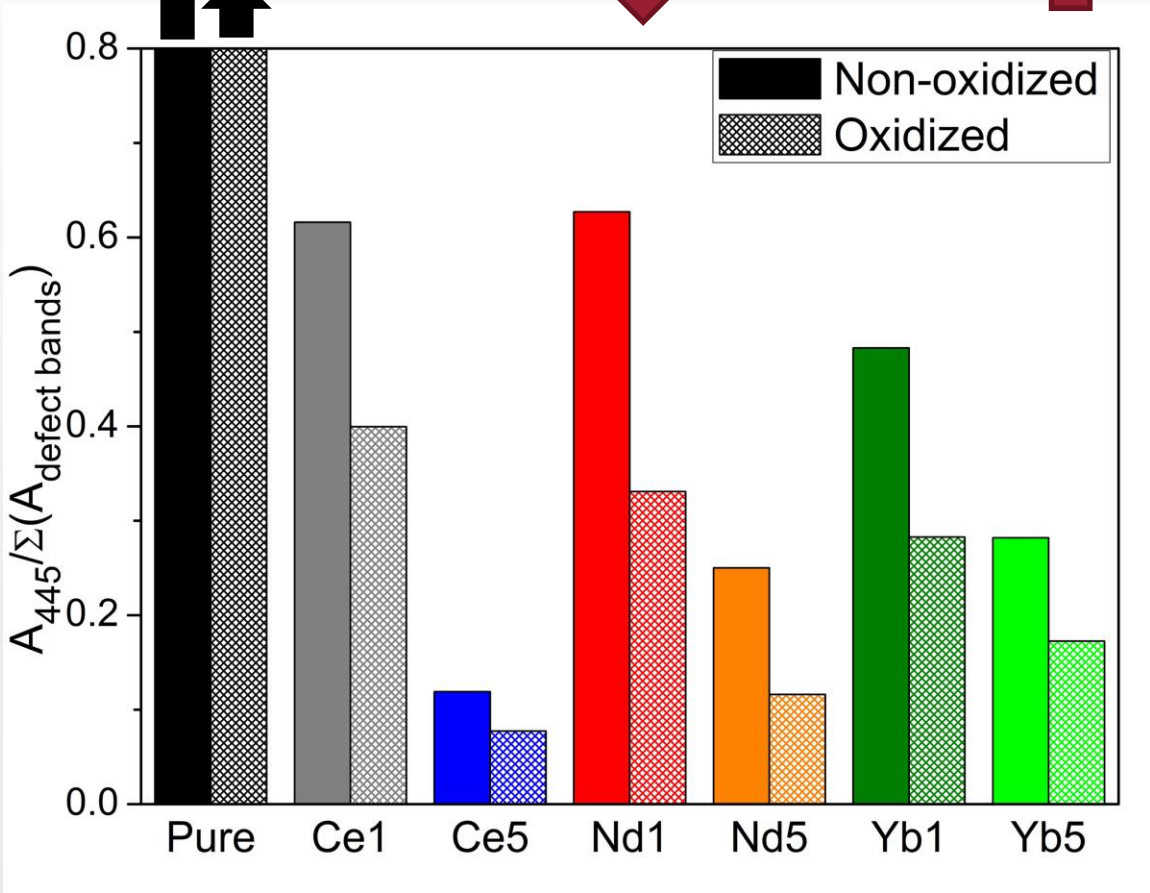

Measured with red laser

Raman - T_{2g}/540 (V_O)

Ratio decreases with increasing dopant concentration, and further decreases after oxidizing

540 band disappears in the pure sample after oxidation, indicating that all oxygen vacancies were filled

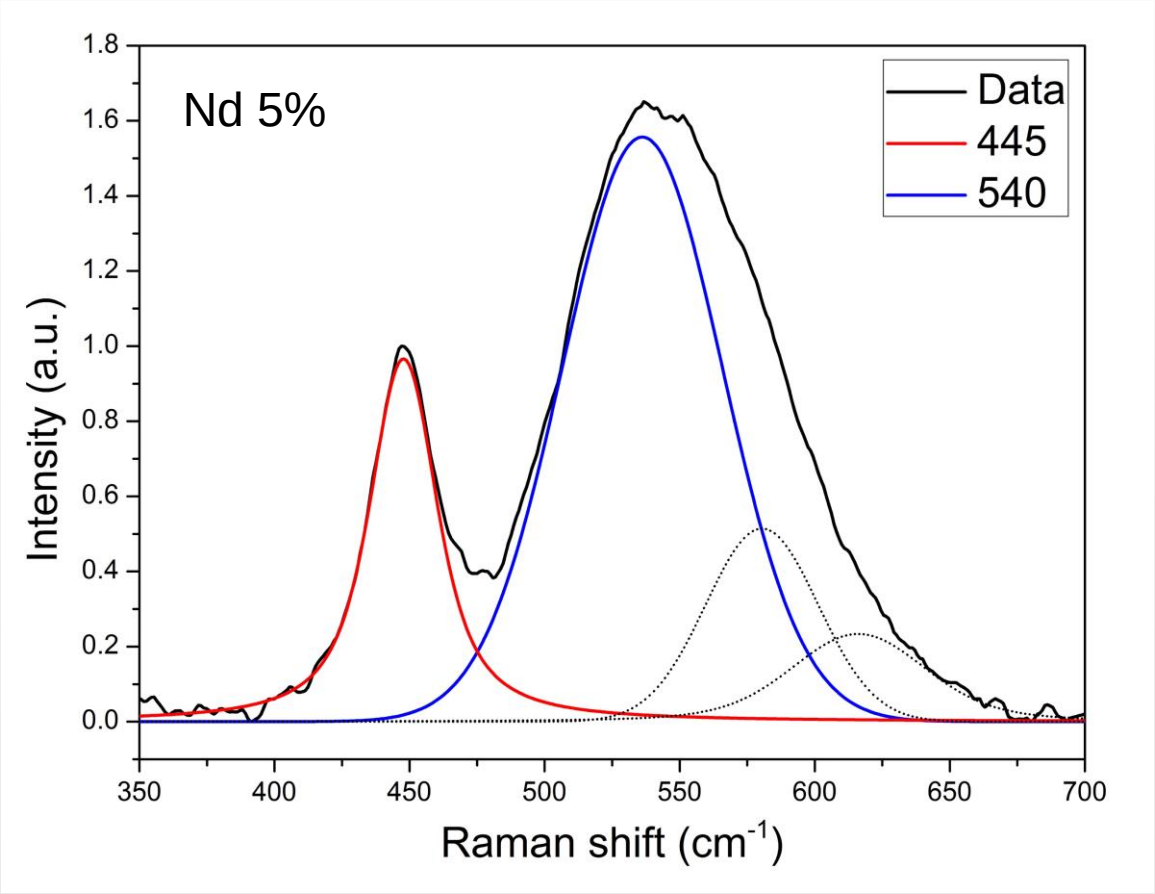

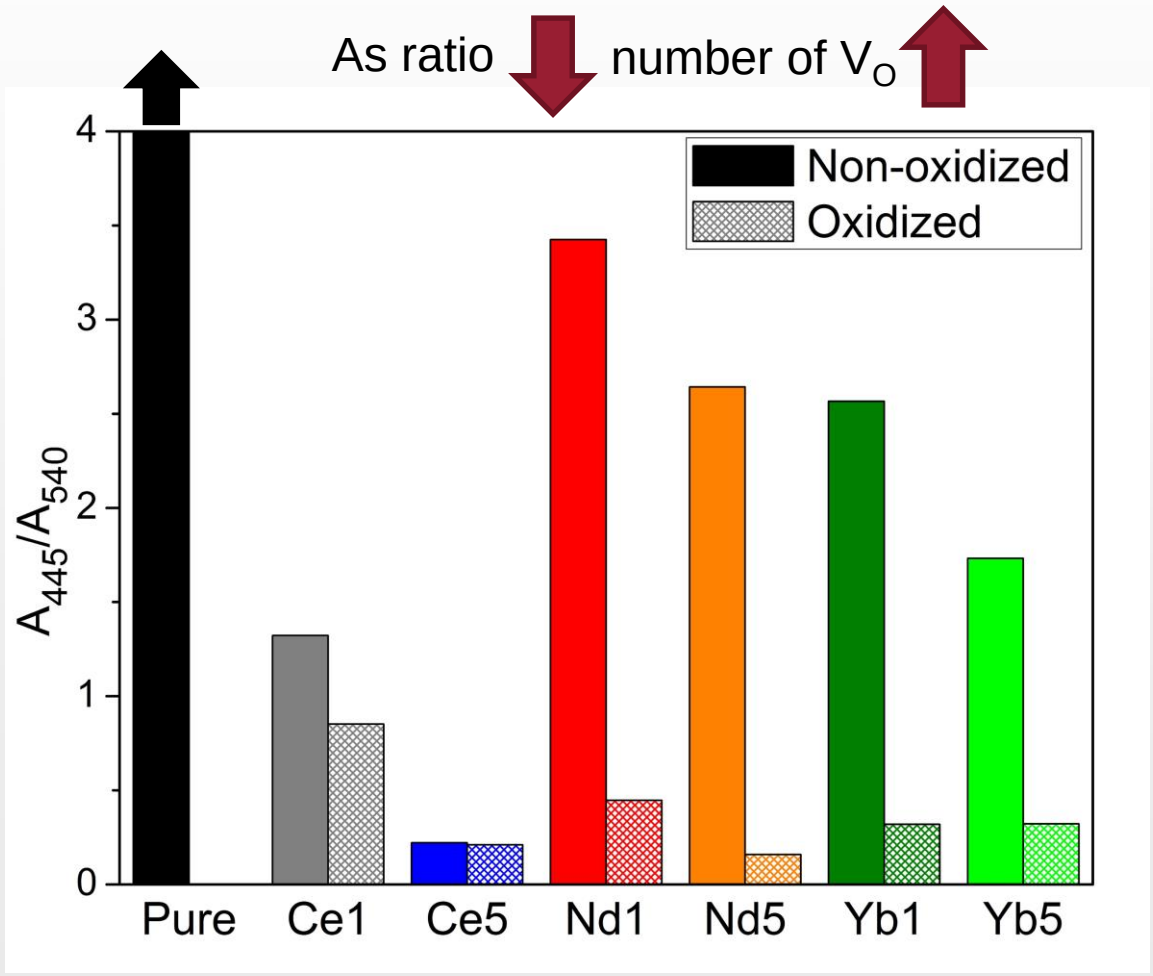

Measured with red laser

Raman - T_{2g}/575 (1LO)

Increasing dopant concentration causes a **loss of symmetry** and **lattice distortion**, 1LO band increases

Ratio **decreases** after oxidation for Ce-doped samples, **increases** for Nd and Yb-doped samples

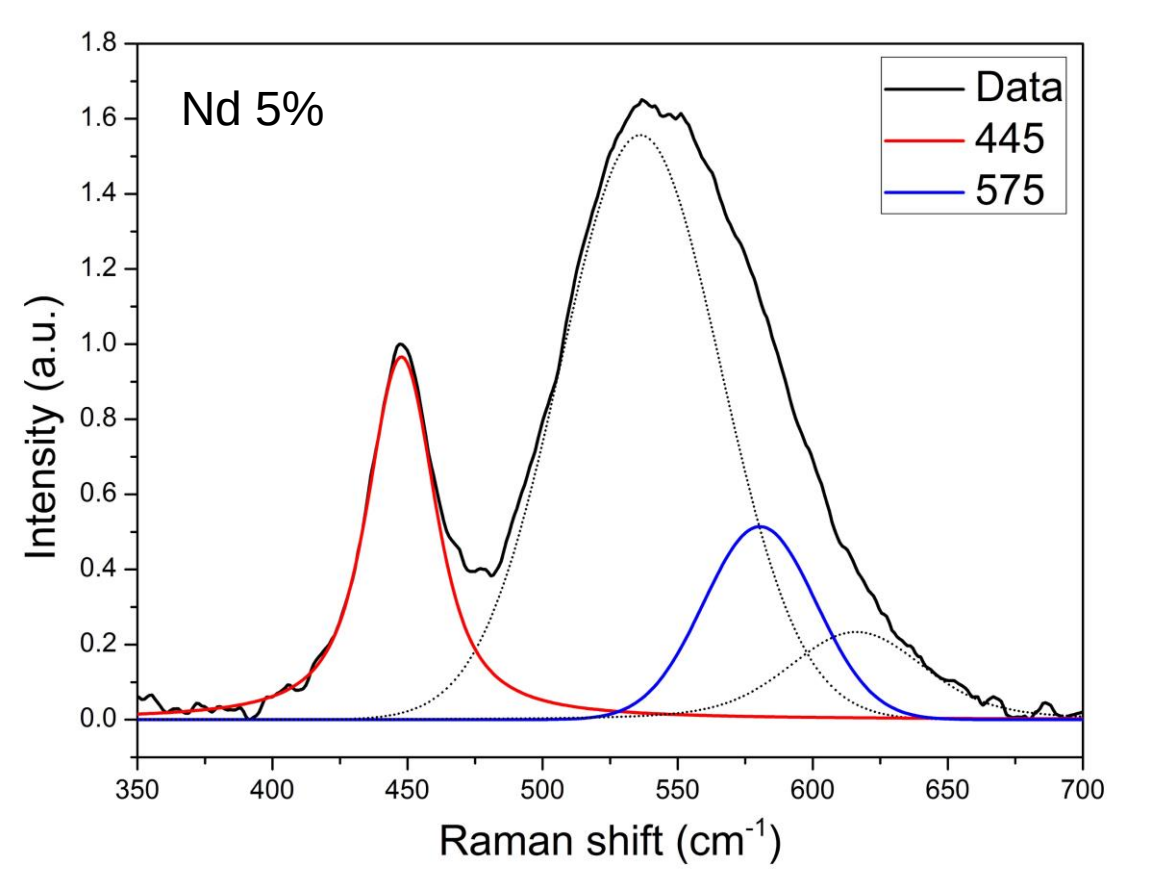

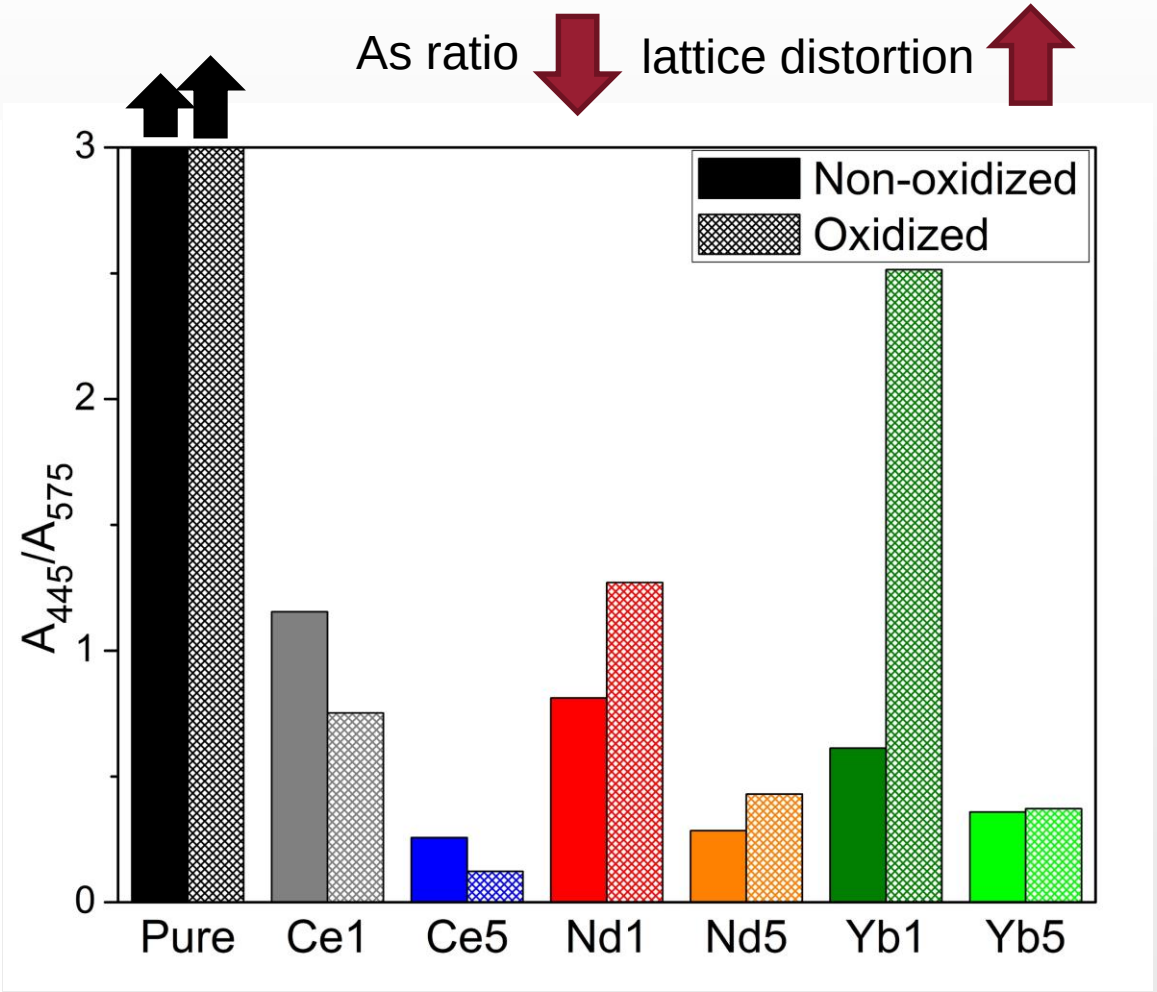

Measured with red laser

Raman - T_{2g}/640 (O clustering)

640 band attributed to a **distortion of the anion sublattice** caused by **interstitial O atoms** related to **U_4O_9 cuboctahedral cluster** formation

640 band not observed in Ce or oxidized doped samples → dopants are effective in inhibiting U_4O_9 formation/oxidation

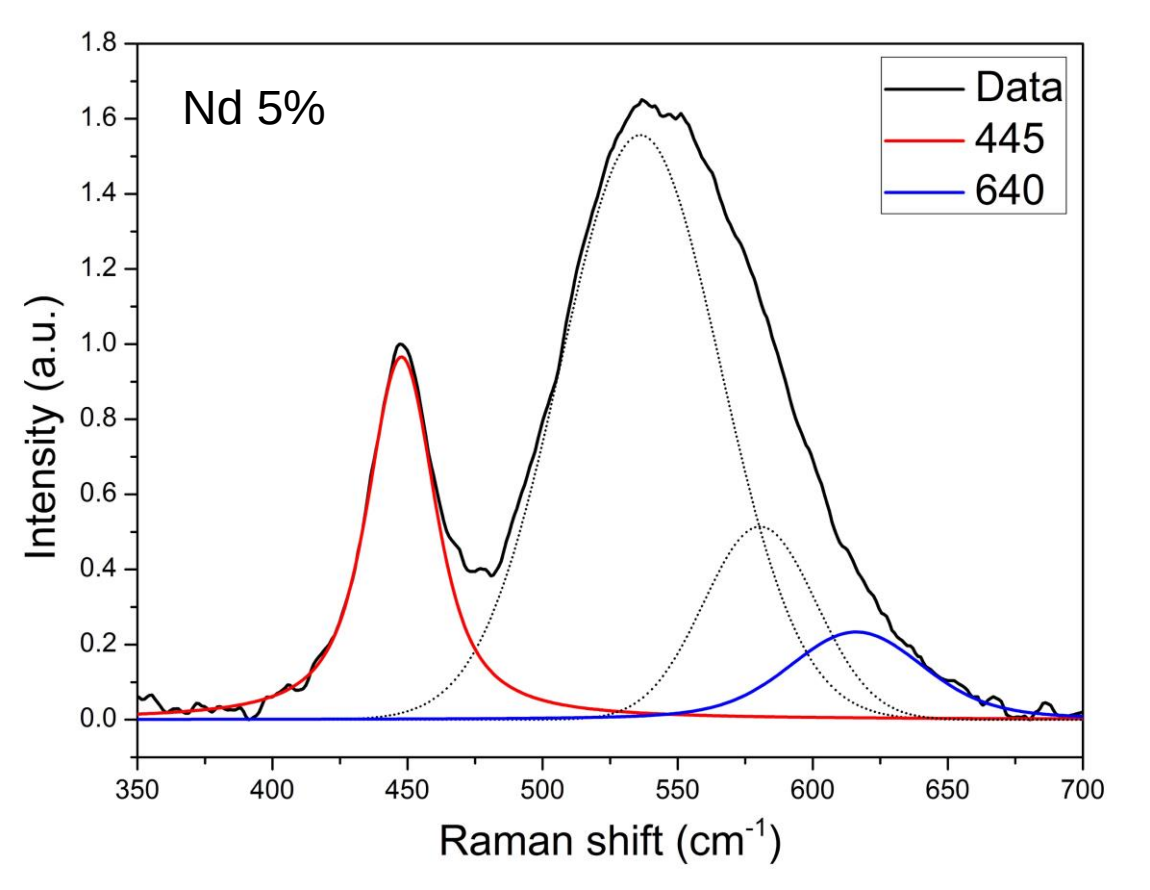

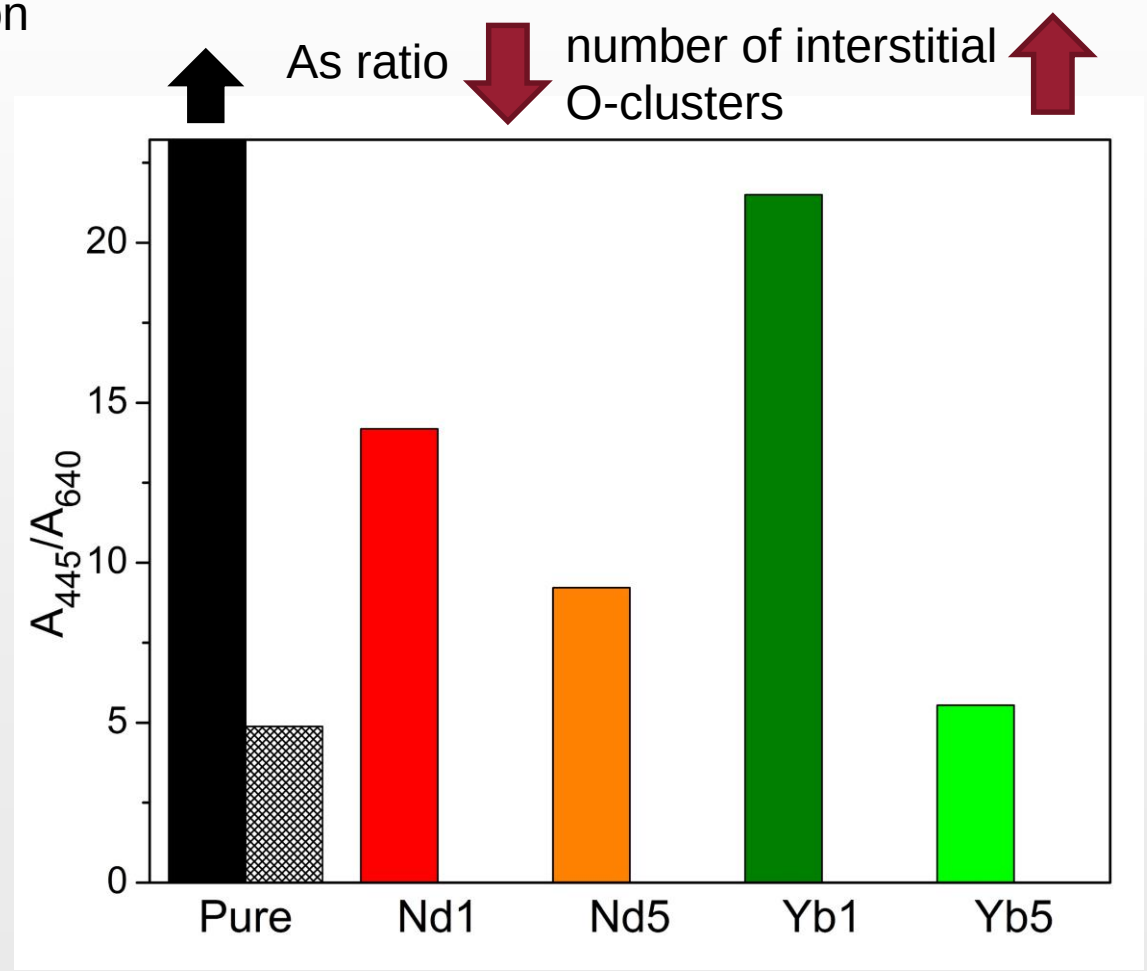

Measured with red laser

Raman - T_{2g}/2LO

Non-stoichiometry leads to a significant decrease in intensity of the 2LO band

"Fingerprint" of undisturbed fluorite lattice structure

As ratio ↑ fluorite lattice structure becomes more distorted

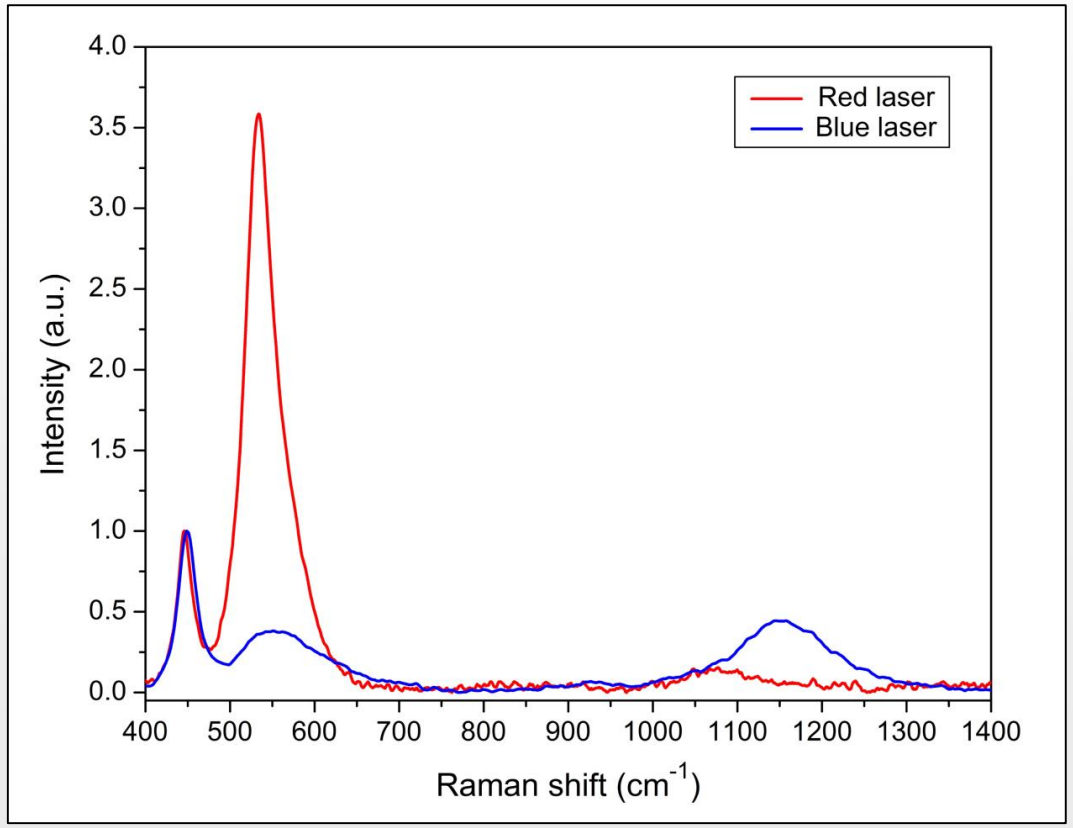

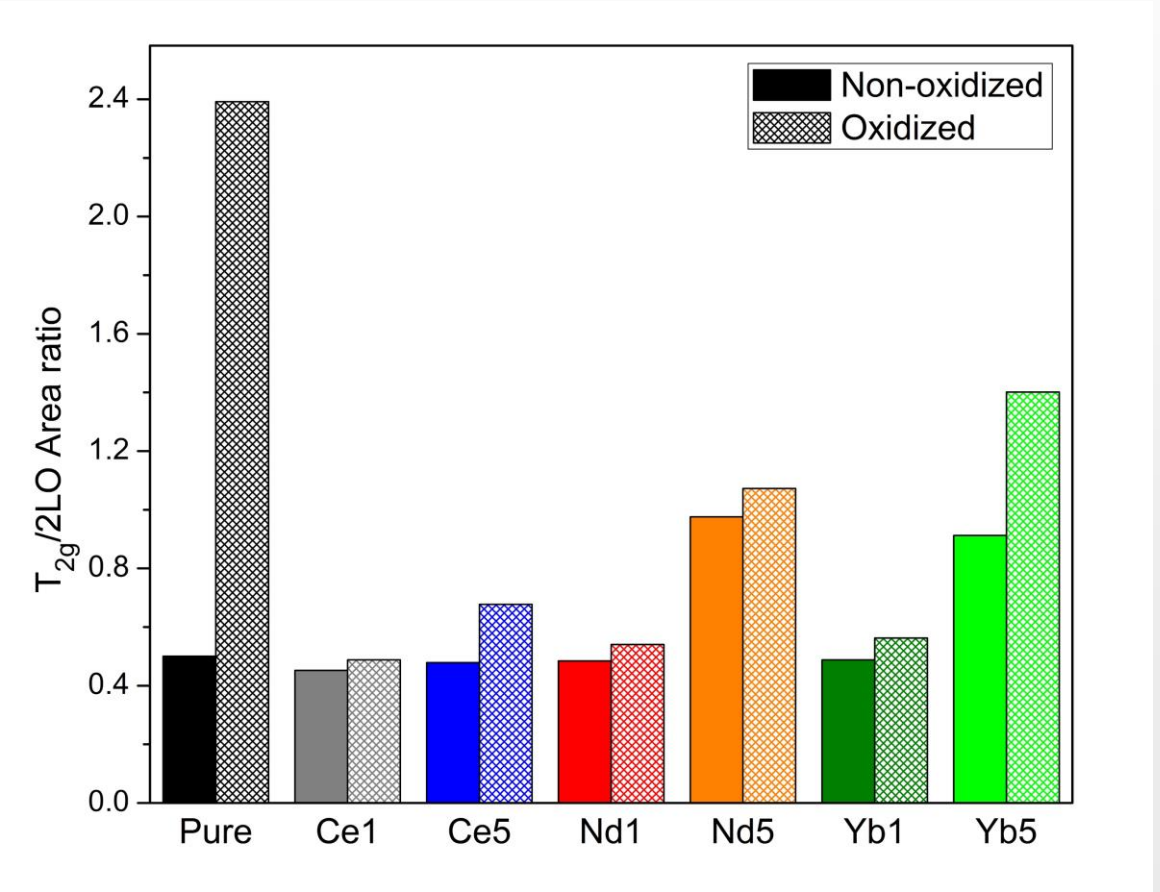

Measured with blue laser

TGA/DSC

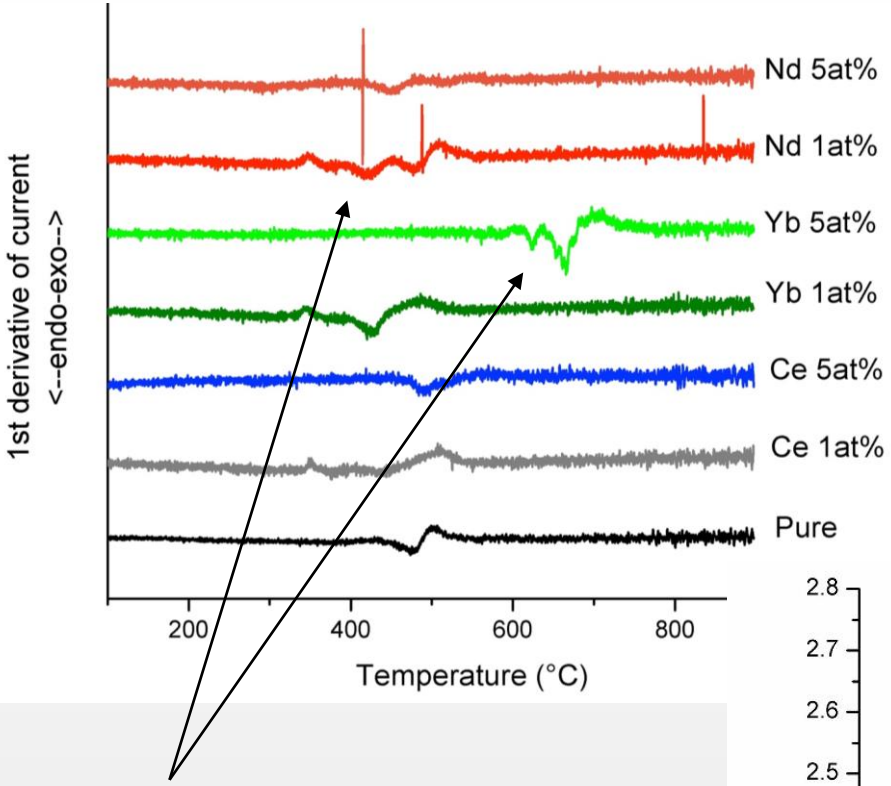

More complex phase changes in Nd, Yb-doped samples

M_{conc} (at%)	$O/(U+M)_{final}$	$(U_{1-y}M_y)_4O_9$: $(U_{1-y}M_y)_3O_8$	Reaction 1 onset T (°C)	Reaction 2 onset T (°C)
Pure	2.66	0.016:0.984	~350	~450
Ce 1	2.65	0.04:0.96	~380	~450
Ce 5	2.67	0:1	~390	~480
Yb 1	2.69	0:1	~300	~390
Yb 5	2.65	0.04:0.96	~530	~620
Nd 1	2.66	0.016:0.984	~300	~400
Nd 5	2.64	0.064:0.936	~250	~410

O/(U+M) ratio

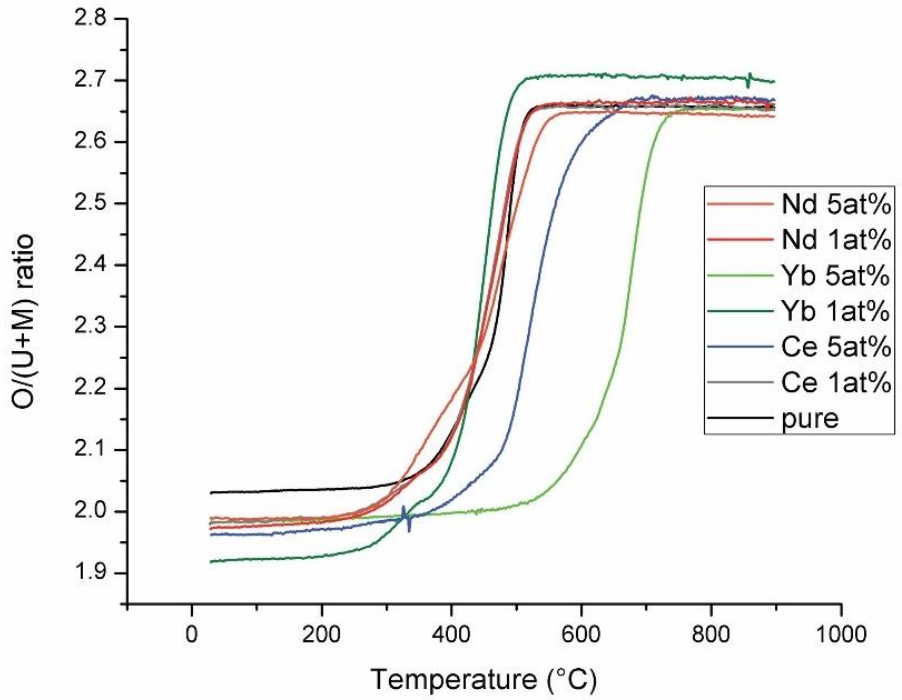

1st derivative of mass gain as a function of temperature from TGA

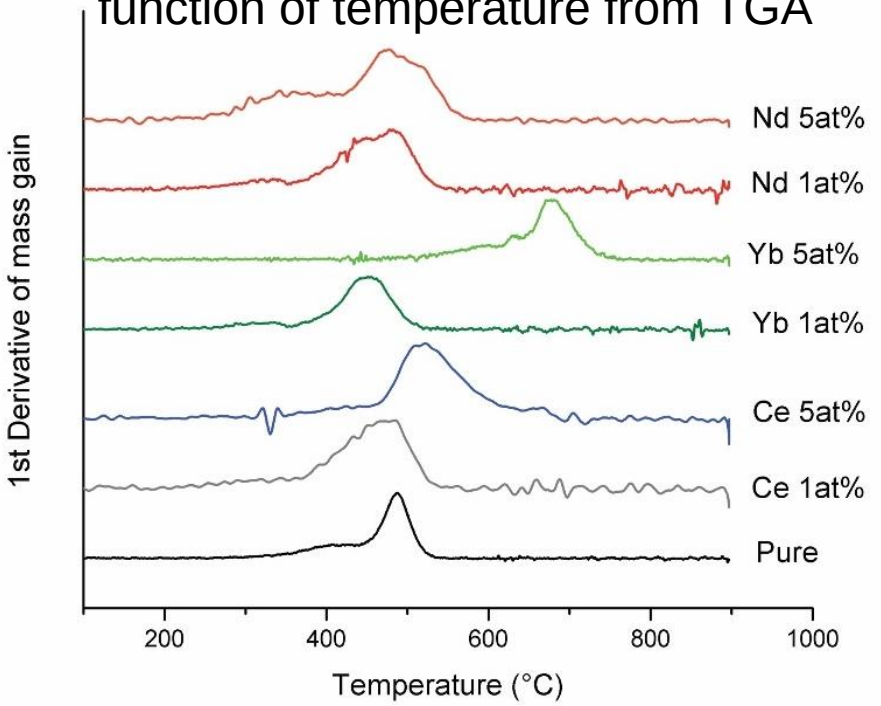

Conclusions and future work

Oxidation delay: Yb → Ce → Nd

	455 nm	785 nm
Better for:	2LO	V_O, 1LO

Deconvolution of Raman spectra reveal different oxidation and defect structure effects from dopants:

- 1LO increases in Ce after oxidation, but decreases in other samples
- But, 2LO decreases more with higher concentration of Nd and Yb

– Explained by difference in dopant size, charge (3+ vs. 3+/4+)?

- More accurate Ce^{III}/Ce^{IV} to help explain 1LO band increase with oxidation
- $U^{IV}/U^{V}/U^{VI}$ ratios
- Hot-stage Raman and XRD measurements
- Th and Zr-doped UO_2 (4+ cation dopants)

How will oxidation and dissolution behavior compare?

SPFT dissolution tests

Acknowledgements

- Dr. Travis Olds, Dr. John McCloy, Dr. Xiaofeng Guo, Kyle Kriegsman
- U.S. Department of Energy in support of the Nuclear Energy University Program – Used Nuclear Fuel Disposition program, award # DE-NE0008689.
- US Department of Energy Office of River Protection for funding through 89304017CEM000001 for purchase of the Raman microscope system used in this work.

NEUP Nuclear Energy University Programs

U.S. Department of Energy

This work is supported by the Nuclear Energy University Program, Office of Nuclear Energy of the U.S. Dept of Energy (# 17-13054).

NOME Materials Laboratory

nuclear optical magnetic electronic

OFFICE OF RIVER PROTECTION

United States Department of Energy